Interaction of shock-waves with a compliant wall

Carmen Riveiro Moreno, Marie Couliou, Nicolo Fabbiane, Olivier Marquet, Reynald Bur

Association Aéronautique et Astronautique de France

57th 3AF International Conference on Applied Aerodynamics
29 — 31 March 2023, Bordeaux – France

AERO2023-86-RIVEIRO MORENO

Interaction of shock-waves with a compliant wall

C. Riveiro Moreno[(1)], M. Couliou[(2)], N. Fabbiane[(3)], O. Marquet[(4)] and R. Bur[(5)]

[(1)]*DAAA, ONERA, Université Paris Saclay, F-92190 Meudon, France, carmen.riveiro_moreno@onera.fr*

[(2)]*DAAA, ONERA, Université Paris Saclay, F-92190 Meudon, France, marie.couliou@onera.fr*

[(3)]*DAAA, ONERA, Université Paris Saclay, F-92322 Châtillon, France, nicolo.fabbiane@onera.fr*

[(4)]*DAAA, ONERA, Université Paris Saclay, F-92190 Meudon, France, olivier.marquet@onera.fr*

[(5)]*DAAA, ONERA, Université Paris Saclay, F-92190 Meudon, France, reynald.bur@onera.fr*

ABSTRACT

The Shock/Boundary Layer Interaction (SBLI) over a rigid plate with an upstream 1.35 Mach number is characterized experimentally by unsteady pressure measurements and schlieren visualizations. Spectral Proper Orthogonal Decomposition (SPOD) is used on the schlieren videos to characterize the flow. The shock displacement spectrum is then used to chose a compliant wall. The interaction of the SBLI the compliant wall is analysed with schlieren imagery. The interaction consists on a lock-in of the flow at the structure's vibration frequency.

1. INTRODUCTION

Shock-waves are inherent to transonic, supersonic and hypersonic regimes, and thus are present in numerous locations in high speed vehicles: aircraft wings, air engine inlets, and control surfaces to name a few. In the presence of sufficiently strong shock-waves, the adverse pressure gradient causes boundary layer separation, prompting an unsteady flow, characterised by low-frequency broadband shock oscillation, two orders of magnitude lower than that of the small-scale structures present in the incoming boundary layer. The resulting unsteady flow can give rise to transonic buffet on wings, buzz on supersonic engine air intakes, and unsteady pressure and thermal loads on the structure among others [7].

Another consequence of Shock/Boundary Layer Interaction (SBLI) dominated flows can be structural fatigue failure. Due to lightweight constrains, high speed vehicles are characterized by the use of thin flexible panels that become compliant under the presence of the flow, that is, they passively deform due to the fluid structure interaction (FSI). In the presence of Shock/Boundary Interaction (SBLI), panels dynamically respond to low frequency pressure fluctuations which can lead to failure due to high-cycle fatigue when the flow couples with the panel's resonance modes. Even if the mechanism behind the SBLI's low frequency fluctuations is not yet fully understood, a significant amount of research has focused on the interaction of flexible thin plates with shock-waves in the last decade.

Experimental campaigns have characterised the SBLI in the presence of an impinging shock [3, 18, 19] as well as compression ramps [10, 1]. In these studies, the dynamics of the flow and the compliant wall were measured using non intrusive techniques such as Digital Image Correlation (DIC), schlieren visualizations, Particle Image Velocimetry (PIV) or Pressure Sensitive Paint (PSP). They investigated the influence on the interaction of shock impingement position and the cavity pressure under the plate [18], thickness of the panel [10], thermal loads and shock strength [3] among others. Works from [10, 1, 15, 19] highlighted the presence of fluid-structure coupling by showing the presence of natural frequency peaks of the compliant wall on the flow spectrum. In their experiment. Brouwer et al.[3] found limit cycle oscillations of the thin plate under the influence of a weak shock.

In transonic flows, investigations on the interaction of a normal shock with a thin metallic plate [13, 14, 12] explored the use of panel deformation to recreate the effect of Shock Control Bumps (SCB)[4]. Even in a bistable behaviour of the shock was observed at large plate deformations [13], the dynamic coupling mechanism is not explained.

The aim of this study is to shed new light in the fluid structure interaction with the presence of a normal shock-wave (transonic regime). For this purpose, the present

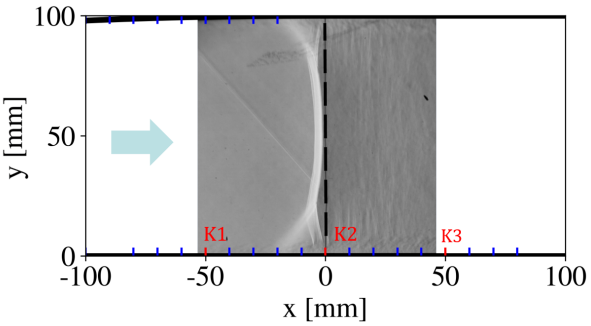

Figure 1: Shock location in test section of S8Ch. In blue are the location of static pressure sensors. In red are the location of the three unsteady pressure sensors (K1, K2, K3)

work focuses on experimentally characterizing the interaction between a compliant wall and a normal unsteady shock with a 1.35 upstream Mach number. Firstly, the interaction of the shock-wave with the incoming turbulent boundary layer on the rigid wall is analysed by unsteady pressure measurements and high speed schlieren imagery. Knowing the dynamics of the flow, a compliant wall is designed so that its natural frequency is of the same order of magnitude as the shock oscillations. Lastly, the fluid structure interaction of the oscillating shock and the compliant wall is studied by high speed schlieren imagery.

2. WIND TUNNEL FACILITY

Experiments are conducted in S8Ch ONERA's transonic open circuit wind tunnel in Meudon. This wind tunnel, has been largely used for experimental studies on passive and active (fluidic) control of SBLI [6]. The stagnation temperature in the settling chamber is 300 ± 10 K and the stagnation pressure 96.0 ± 0.3 kPa.

For this study, S8Ch is equipped with a half nozzle that generates an unsteady normal shock-wave with a nominal upstream Mach number of 1.4. The flow is chocked by means of a second throat located at the outlet which isolates the test section from downstream perturbations. By regulating the cross section of the second throat, it is possible to adjust the position of the shock in the channel. The test section's span is 120 mm, its height 100 mm and the end of the nozzle is located at 369 mm from the end of the converging part of the channel. All throughout the experimental campaign, the shock was located at 370 mm from the end of the converging part of the channel, which will be considered as location $x = 0$ as shown in Fig. 1. At this location, the Mach number upstream the shock is equal to 1.35.

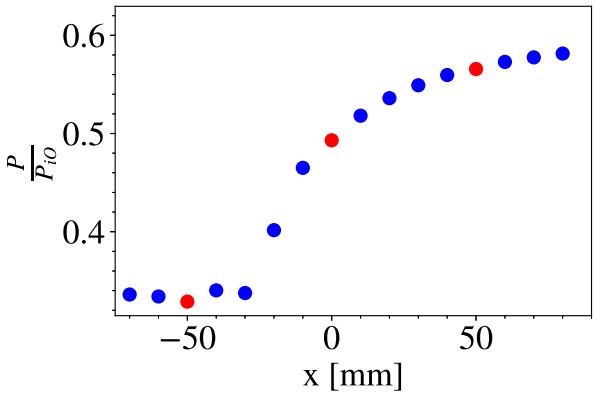

Figure 2: Pressure ratio profile along lower wall of the test section. Red dots correspond to the location of the unsteady pressure sensors. Blue dots correspond to the static pressure sensors.

3. SHOCK-WAVES OSCILLATION

3.1 Pressure wall measurements

Pressure is measured on the centerline of the bottom wall using 30 static pressure sensors and 3 unsteady pressure sensors as illustrated in Fig. 1. The three unsteady pressure sensors are Kulite transducers type XCQ-093-15A which sampled pressure fluctuations at 100kHz for 60 s with a high pass filter at 10kHz.

Fig. 2 shows the pressure ratio P/P_{i0} along the lower wall of the test section, where the red dots indicated the time-averaged measurements made with the unsteady pressure sensors and the blue dots correspond to the static pressure measurements. This pressure distribution reveals the high adverse pressure gradient the normal shock imposes on the flow. At the location of the shock (x = 0 mm), no pressure plateau is visible meaning that the shock does not induce a massive separation or recirculating flow.

To confirm that purpose, oil visualizations were conducted, and it was found, that there exists only a small separation bubble around the centerline of the test section's lower wall. The existence of this incipient separation is consistent with the notion that the onset of shock-induced separation that is expected for Mach numbers ranging from 1.3 to 1.35 [2].

From Fig. 1, it can be seen that solely the center unsteady pressure sensor named K2 is located at the rear leg of the shock foot. The other two pressure sensors K1, K3 are located further upstream and downstream (respectively 50 mm upstream and downstream K2 location.).

In order to capture the pressure dynamics along the shock foot and add locations of dynamic pressure measurements, the shock is displaced 21.4 mm downstream and then 11.4 mm upstream, which is equivalent to add two pressure measurement locations named respectably

K2' and K2". As the Mach number upstream of the shock is only sightly modified, the physics of the flow remains unchanged, especially the boundary layer separation region. As a result, one has access to the unsteady pressure measurement at 5 positions as visible in Fig. 3. The first unsteady sensor, K1 is located in the incoming boundary layer, K2' is under the shock foot, K2 within the separation region, K2" is at reattachment and K3 is further downstream of the interaction region.

Fig. 3 displays the premultiplied spectra for the unsteady pressure measurements at these five locations. The spectra were obtained through the Welch method using 24576 samples per block, and a Hanning windowing with a 50% of overlap. Low frequency oscillations, below 20 Hz, were found to be the result of fluctuations of the stagnation pressure in the settling chamber. Consequently, the spectra below 20 Hz is cut out in Fig. 3.

The premultiplied spectrum of the pressure at the location K1 (Fig. 3a) shows a high frequency bump with its maximum around 8kHz. We associate it to the high frequency pressure fluctuations caused by the small structures contained in the incoming boundary layer. Note that the amplitude of the oscillations is two orders of magnitude lower than the other spectra that will be presented.

Under the first leg of the shock foot, the premultiplied spectrum (K2', Fig. 3b) shows a low frequency bump centered around 200 Hz. This spectrum is representative of the shock oscillations. The lack of high frequencies on the spectrum as the one present on the incoming boundary layer (Fig. 3a), suggests that the shock behaves as a low pass filter with a cut off frequency around 200 Hz. Additionally, it can be seen that amplitude of the shock oscillations are the highest of all spectra presented in Fig. 3.

Within the separation region, the premultiplied spectrum of K2 (Fig. 3c), shows a broad low frequency bump accompanied by a high frequency bump located around 6kHz. As the flow undergoes the extreme pressure gradient because of the front leg of the shock, the flow detaches generating a recirculating zone with a mixing layer developing on top of it. The appearance of this high frequency bump in Fig. 3c can be linked to the footprint of the small structures of the mixing layer [7]. On the other hand, the low frequency content can be attributed to the motion of the shock. Note that the energy of the low frequency oscillations is lower than the one obtained under the shock foot (K2', Fig. 3b). These results, suggest that in the recirculating region, where K2 is placed, both the influence of the shock oscillations as well as that of the mixing layer coexist [16].

At the reattachment region, the premultiplied spectrum, represented by K2" in Fig. 3d, consists in a high frequency bump centered at 6kHz. The high frequency bump is the same as the one found in the spectrum of K2 (Fig. 3c), but with higher amplitude. As the boundary layer reattaches, the structures in the mixing layer are brought closer to the wall, which increases the pressure fluctuations felt at the wall. This could account for the increase in amplitude of the high frequency bump observed in Fig. 3d. At the location K2", the amplitude of the low frequency oscillations has decreased with respect to the K2, indicating that there is little influence of the shock oscillations at the reattachment point.

Further downstream of the interaction, the premultiplied spectrum obtained from K3 (Fig. 3e), displays a high frequency bump located at 6kHz. This is the same high frequency bump as in K2 and K2" (Fig. 3c-d). Therefore, the bump is still related to the structures in the mixing layer, which can be felt downstream the interaction. It can be noted that its amplitude has increased with respect to K2". The reason behind comes from the spatial development of the structures shed in the mixing layer as they move downstream. As they become larger, so will the pressure fluctuation associated with it. Hence, the reason for the increase in amplitude of the high frequency bump in Fig. 3e. Same trends have been found in other experimental studies in transonic flow [16], and even in different configurations such as shocks generated by a compression ramp [11] or shock generators [8].

3.2 High speed Schlieren visualizations

Schlieren visualizations are conducted with a Z-type Schlieren setup with a high speed Phantom camera and a blue LED source. A vertical knife orientation was used, which yields images whose light intensity is proportional to horizontal density gradients.

The schlieren image in Fig. 4 presents an instantaneous image of the flow in a zoom region around the shock. In it, it is possible to observe a normal shock with its λ shaped shock foot, which hints the presence of shock induced separation. Note that the apparent thickness of the shock is due to a spanwise integration of light. The horizontal density gradients reveal the shock as well as the shocklets downstream the shock foot, which appear in white, indicating a positive density gradient. The presence of shocklets indicates the existence of secondary supersonic regions downstream of the lambda region [2]. The alternating areas of positive and negative gradients downstream of the shock foot correspond to structures developing in the mixing layer. These structures seem to generate noise that can be seen in the shape of vertical lines right above them, downstream the shocklets.

Spectram Proper Orthogonal Decomposition (SPOD) [17] is computed on the schlieren images with the purpose of finding oscillating coherent structures in the flow, and link them to the findings obtained with the unsteady pressure sensors.

Due to camera memory limitations, it was not possible to obtain a long video of the whole flow field sampled at a high frequency, so that both the low and high frequency

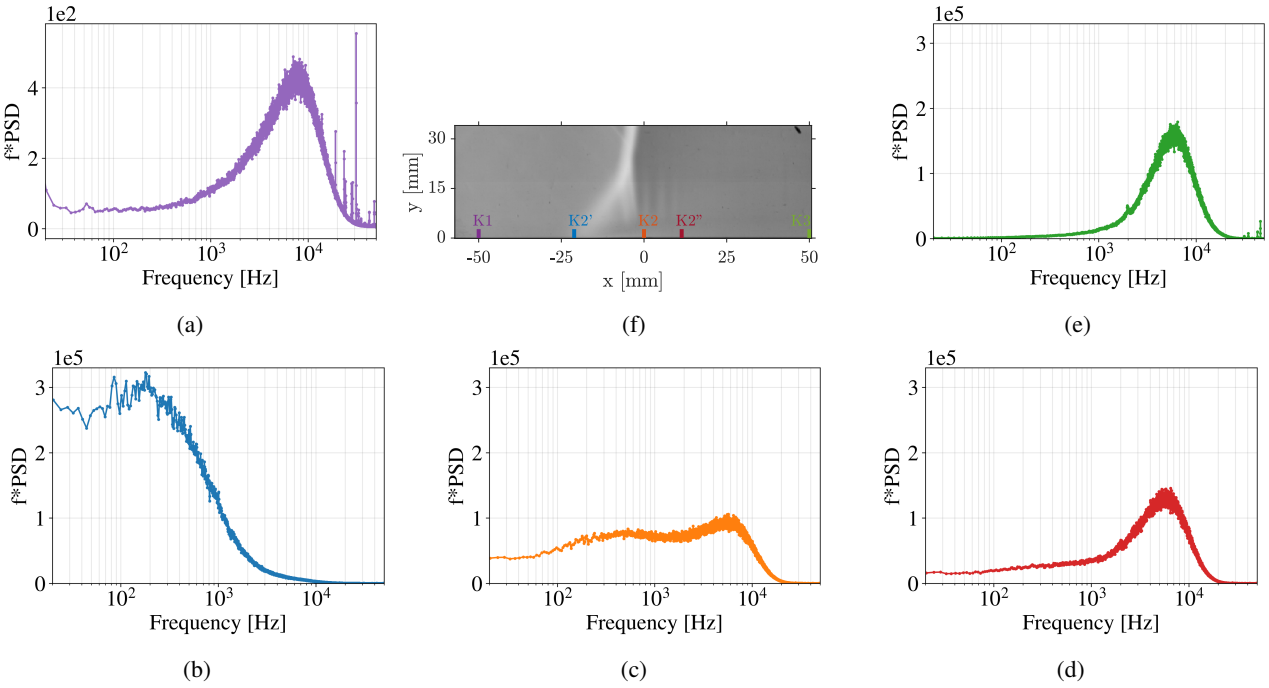

Figure 3: Premultiplied spectra from unsteady pressure sensor at the position a) K1 = - 50 mm (purple), b) K2' = -21.4 mm (blue), c) K2 = 0 mm (orange), d) K2" = 11.4 mm (red) and e) K3 = 50 mm (green). f) Sketch of the pressure sensors localisation superimposed with a Schlieren visualisation

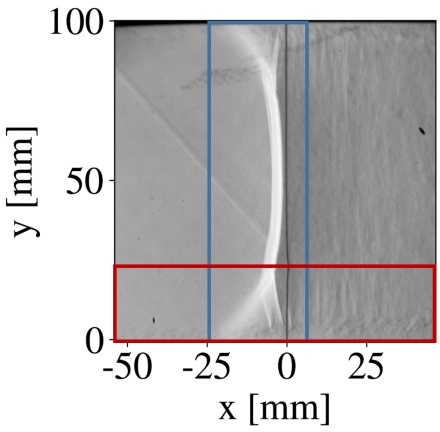

Figure 4: Data sets of schlieren visualization of horizontal density gradients framed at the shock (blue) and at the shock foot (red).

content of the flow, already displayed in Fig. 3, could be captured. Consequently, two different set of images were acquired. The first set was framed at the shock (Fig. 4, blue frame), which has associated low frequencies as seen from the spectrum under the shock foot (Fig. 3b). These videos were acquired at a sampling frequency of 7kHz for a duration of 16.6 s. Another set of images, framed at the shock foot (Fig. 4, red frame), where higher frequency content is expected as seen in the spectra at the recirculation region and downstream of it (Fig. 3), were sampled at 20kHz for 5.8 s. Both set of images have a magnification ratio of 445 pixel to 1 mm, and the image size are of 160x448 pixels in the shock framed images and 480x152 in the shock foot framed images.

In the SPOD calculation, 112 blocks of 2048 samples with a 50% of overlap were used for the shock framed videos, and 55 blocks of 4096 samples with a 50% of overlap for the shock foot framed one. In this manner, the frequency resolution for both calculations is similar, being 3.41 Hz and 4.88 Hz respectively, while ensure a sufficient amount of blocks for convergence of the SPOD computation.

The black line in Fig. 5a presents the premultiplied spectrum of the first eigenvalue for the image data set framed at the shock (Fig. 4, blue frame). Being the first eigenvalue the most energetic, it is therefore the most representative of the flow dynamics. The spectra below 20 Hz is cut out not to display the low frequency oscillations, which are due to fluctuations of the stagnation pressure in the settling chamber. The spectrum for this set of images consists in a low frequency bump.

For a given frequency, the complex eigenvector of the first eigenvalue (from here onwards referred as the first mode) indicates which areas in the flow move coherently with the most energy. So as to analyse which areas of the flow oscillate at low frequency, the first mode at frequencies within the low frequency bump were extracted and

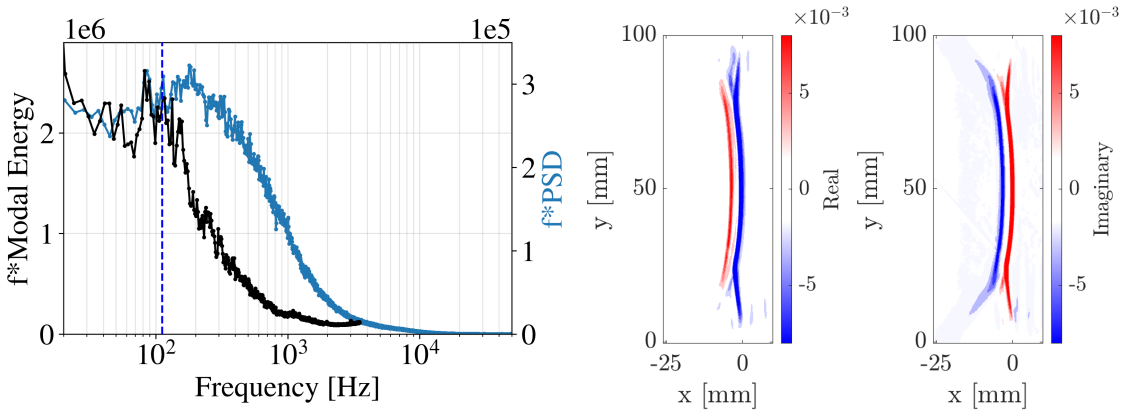

(a) (b)

Figure 5: (a) Premultiplied spectra of first eigenvalue obtained with SPOD for frame centered at the shock (black) (Fig. 4, blue frame) and from the unsteady pressure sensor located at the position K2' under the shock foot (blue). Blue dashed line corresponds to frequency 112 Hz. (b) Real (left) and imaginary (right) parts of the mode for the first eigenvalue at a frequency of 112 Hz.

analysed. Fig. 5b presents the real and imaginary parts of the mode at a frequency of 112 Hz (Fig. 5a, vertical dashed blue line).

When compared to the schlieren image (Fig. 4), it can be inferred that the real and imaginary parts of the mode are located on the shock and to a lesser extend on the shocklets downstream of the shock foot. This implies that the shock presents a pure oscillation. It moves as a rigid structure around an average position. Consequently, it confirms the notion that the pressure spectrum at the shock foot (position K2', Fig. 3b) is representative of the shock motion.

The two areas at the shock on the real and imaginary parts correspond to the most upstream and downstream position of the shock during its oscillation (Fig. 5b). Same patterns and conclusion can be made for the shocklets. Their motion consist on an upstream-downstream translation, synchronized with that of the shock.

Same results were obtained at different frequencies within the bump. Hence, these results confirms the notion that the shock oscillations are broadband and low frequency, as presented in the results of the pressure spectrum (Fig. 5a, blue line). Nonetheless, the low frequency oscillations on the pressure spectrum are broader with respect to the ones obtained with SPOD. The differences with respect to the unsteady pressure sensor are due to the different nature of both measurement techniques.

The premultiplied spectrum of the first eigenvalue for the data set focused at the shock foot (Fig. 4, red frame), is presented in Fig. 6 (black line) along side the pressure spectrum at the reattachment (position K2", Fig. 3d) plotted in red for comparison purposes. For this type of image, spectrum displays a low frequency bump as well as high frequency peaks

At frequencies within the low frequency bump, the real

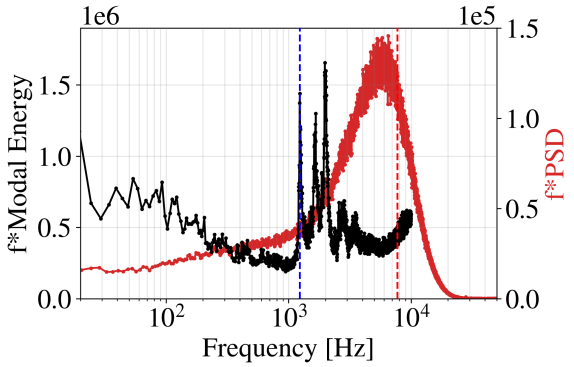

Figure 6: Premultiplied spectrum of first eigenvalue obtained with SPOD for frame centered at the shock foot (black) (Fig. 4, red frame) and of the pressure sensor located at the position K2" in the reattachment region (red). Blue dashed line corresponds to frequency 1235 Hz. Red dashed line corresponds to frequency 7749 Hz

and imaginary parts of the mode show a pure oscillation of the shock foot and at the shocklets, similarly to the real and imaginary parts displayed in Fig. 5b. Thus, it is not presented for brevity reasons.

On the higher frequency part of the spectrum, it is worth noticing the existence of three distinctive peaks at frequencies 1235 Hz (Fig. 6, vertical dashed blue line), 1665 Hz and 1977 Hz on the spectrum. The real and imaginary parts of the first mode at frequency 1235 Hz (Fig. 7a) are located mainly downstream the shock, above the boundary layer. Within this region, the real and imaginary parts are not coincident. This suggests the presence of upstream traveling waves, which could be linked to upstream acoustic propagation. Traveling waves above the mixing layer are also found on the modes at the other two

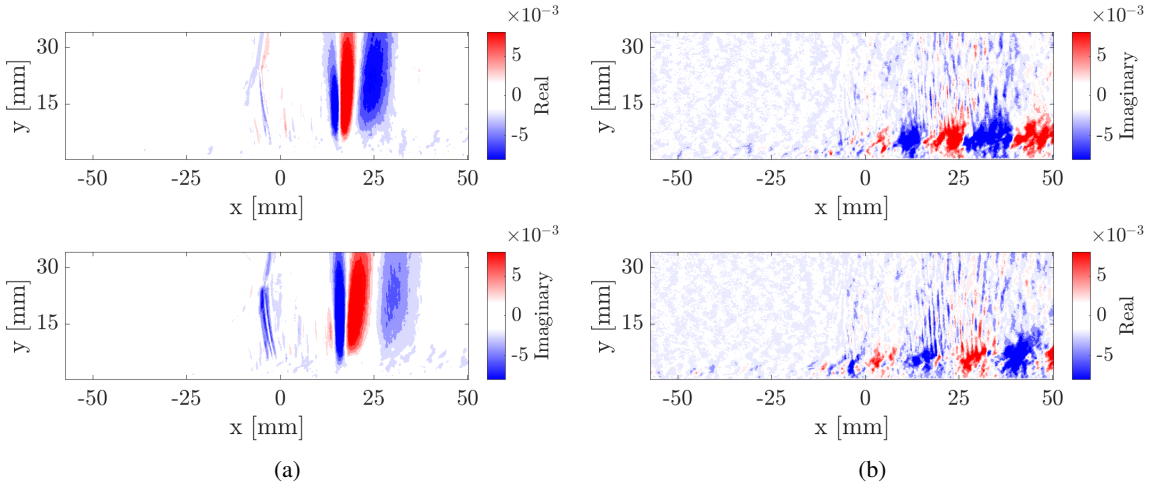

Figure 7: SPOD's real (top) and imaginary (bottom) parts of the mode for the first eigenvalue at a frequency of a) 1235 Hz and b) 7749 Hz.

peaks (1665 Hz and 1977 Hz) as well as the two consecutive bumps below 4kHz. These peaks and bumps are not present on the pressure spectra obtained within the reattachment area (position K2", Fig. 3d) nor in locations further downstream (position K3, Fig. 3e). Being the sensors under the mixing layer and the upstream traveling waves located above it, the pressure sensors do not detect the acoustic waves, or at least, their influence at the boundary layer is not strong enough to overcome the pressure fluctuations coming from the mixing layer.

On the real and imaginary parts at frequency 1235 Hz (Fig. 7a) it is also possible to observe part of the shock foot. As the flow downstream the shock is subsonic, it is possible for downstream pressure perturbations to propagate upstream and interact with the shock, affecting its position and strength. Numerous studies have been conducted on the influence of downstream perturbation generated by a rotating shaft, that generates quasi-sinusoidal pressure signals, on the dynamics of the shock in transonic flow [9, 5, 4]. All coincide that, as the frequency of the shaft was increased, keeping pressure oscillation constant, the amplitude of the shock displacement decreased. Therefore, even if on the first mode's real and imaginary parts there is an area concerning the shock, its oscillation amplitude is smaller than for lower frequencies. This explains why high frequency peaks related to acoustic perturbations are not present in the unsteady pressure spectrum obtained at the shock foot (Fig. 5a, blue). Additionally, as the location of the upstream traveling waves are cut out of the image frame, these peaks are not present on the SPOD results with the image data set focused on the shock (Fig. 5a, black).

At higher frequencies, above 4KHz, as illustrated by the first mode extracted at frequency 7749 Hz (Fig. 6, vertical dashed red line), the real and imaginary parts are located downstream, in the region coinciding with the mixing layer and on the flow immediately above (Fig. 7b). As the real and imaginary parts are not coincident, it suggests that there is a traveling motion of structures contained in the mixing layer. It seems therefore, that there is a propagation of vortical structures that spatially develop as they move downstream. Judging by their vortical shape, at this level of frequency, these structures could be the result of a Kelvin-Helmholz instability.

These results are consistent with the pressure spectra obtained within the separation region and further downstream i.e from K2 to K3 (Fig. 3c to Fig. 3e). The high frequency bump present in these spectra, related to the mixing layer, is of the same order of magnitude as the frequency range where these vortical structures in the mixing layer are present on the first mode. Furthermore, the increase in size of the vortical structures as the move downstream is coherent with the increment on the high frequency amplitude observed from K2' to K3 (Fig. 3, red, green).

The coherent vertical lines above the vortices presented in the real and imaginary parts of the mode (Fig. 7b) are probably related to noise radiation from the mixing layer.

	Incoming BL	Shock	Mix. layer
Freq. (kHz)	[5, 10]	[0.07, 0.3]	[4, 8]
$(\text{f*PSD})_{\text{max}}$	5×10^2	3.3×10^5	1.7×10^5

Table 1: Summary of frequency content in the shock boundary layer interaction

The interaction of the shock with the incoming boundary layer developing on a rigid wall is characterized by several flow phenomena at different time scales, as sum-

marized in Tab. 1. The frequencies characterizing the shock oscillation are lower than those existing in the incoming boundary layer or in the shear layer downstream the shock.

4. INTERACTION OF A SHOCK WAVE WITH A COMPLIANT WALL

We are now interested in analysing the interaction of the shock with a compliant wall. With that aim, the latter will be designed so that its vibration modes of lowest frequency lie in the range of frequencies where the shock oscillates, i.e. between 70 Hz and 300 Hz as shown in Tab. 1.

4.1 Description of the compliant wall

The compliant wall is made of a polyurethane block that is inserted in an aluminium container. The elastic properties of the polyurethane were characterized with a rehometer giving a Young modulus equal to 3 MPa. This material is clamped to the four lateral surfaces of the container but is free to move at the bottom and top surfaces, the latter being the interface with the flow. The compliant wall is 160 mm long, 85 mm wide, and 20 mm thick. As shown later, this thickness allows the lowest natural vibration modes of the compliant wall to be between 100 - 200 Hz, i.e. in the range of frequency characterizing the shock oscillation. As shown in the picture of Fig. 8, the container is placed on the lower wall of the test section. Its mid point coincides with the location of the shock, denoted as $x = 0$ in Fig. 1. In the experiment described below, the shock will be therefore located at the center of the compliant wall, as shown in the sketch of Fig. 8. Finally, it should be noted that, under the compliant wall, the pressure is not equal to the atmospheric pressure, but rather corresponds to an average value of the pressure upstream and downstream the shock, due to leaks (mechanical joints, gaps, ...) in the test section of the wind tunnel.

4.2 Experimental analysis of the shock-wave/compliant-wall interaction

The schlieren images are first used to study the interaction of the compliant wall with the shock wave. They are sampled at 7 kHz for a duration of 3.87 s. Their width is here increased to view the entire length of the compliant wall. Moreover, a vertical knife orientation is used so that only the horizontal density gradients are retrieved.

Fig. 9 displays a series of instantaneous schlieren visualizations of the interaction of the shock with the compliant wall ($t_n, n = [1,5]$), as well as a snapshot of the rigid wall for comparison purposes. On the interaction

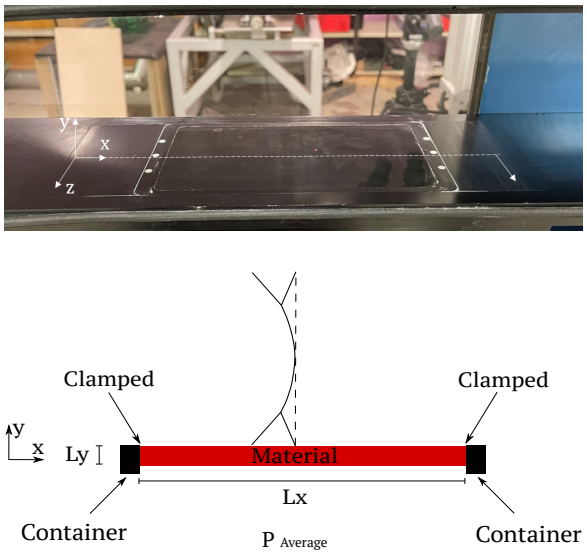

Figure 8: View of the compliant wall on the lower wall of the test section (top). Sketch of a lateral view along the center line (white dashed line on top image) of the compliant wall with the location of the shock (bottom)

with the compliant wall, we clearly observe an oscillation of the shock position as well as a large displacement of the wall. An upwards displacement of the later is represented by a dark zone in the schlieren image due to the shadow projected by the wall onto the camera plane. On the other hand, the downward motion of the wall is not visible due to the nature of the setup. The first schlieren image (Fig. 9, t_1) displays an upward deformation of the wall between $x = -80$ mm and $x = 0$ mm with a maximum located around $x = -40$ mm. At this instant, the shock is located at $x = 0$ mm and it is non symmetric with a large λ shape, indicating the existence of a large separation region. Note that the shock foot shape on the rigid wall case is smaller. The instant t_2 shows that the upward deformation of the wall has decreased and the shock has undergone an upstream motion. It can also be noted that the shock foot has reduced in size, which suggests a smaller recirculating bubble underneath the shock foot. The schlieren image at t_3 presents no visible upward deformation at the wall and a flow similar to the snapshot at t_2 . Later at t_4, while upstream the shock there is no visible displacement of the compliant wall, an upward deformation can be observed from 0 to 80 mm, with a maximum around 40 mm. The flow displayed in the schlieren image at t_4 presents a more symmetric shock with a smaller λ region and small structures being shed downstream. The topology of the shock at this instant resembles that found in the rigid case. At t_5, no deformation is observed at the wall indicating that the deformation from x = 0 to x = 80 mm has decreased. The shock is still around the same position as on the snapshots from t_2 to t_4 and the flow resembles that at instant t_4. On the

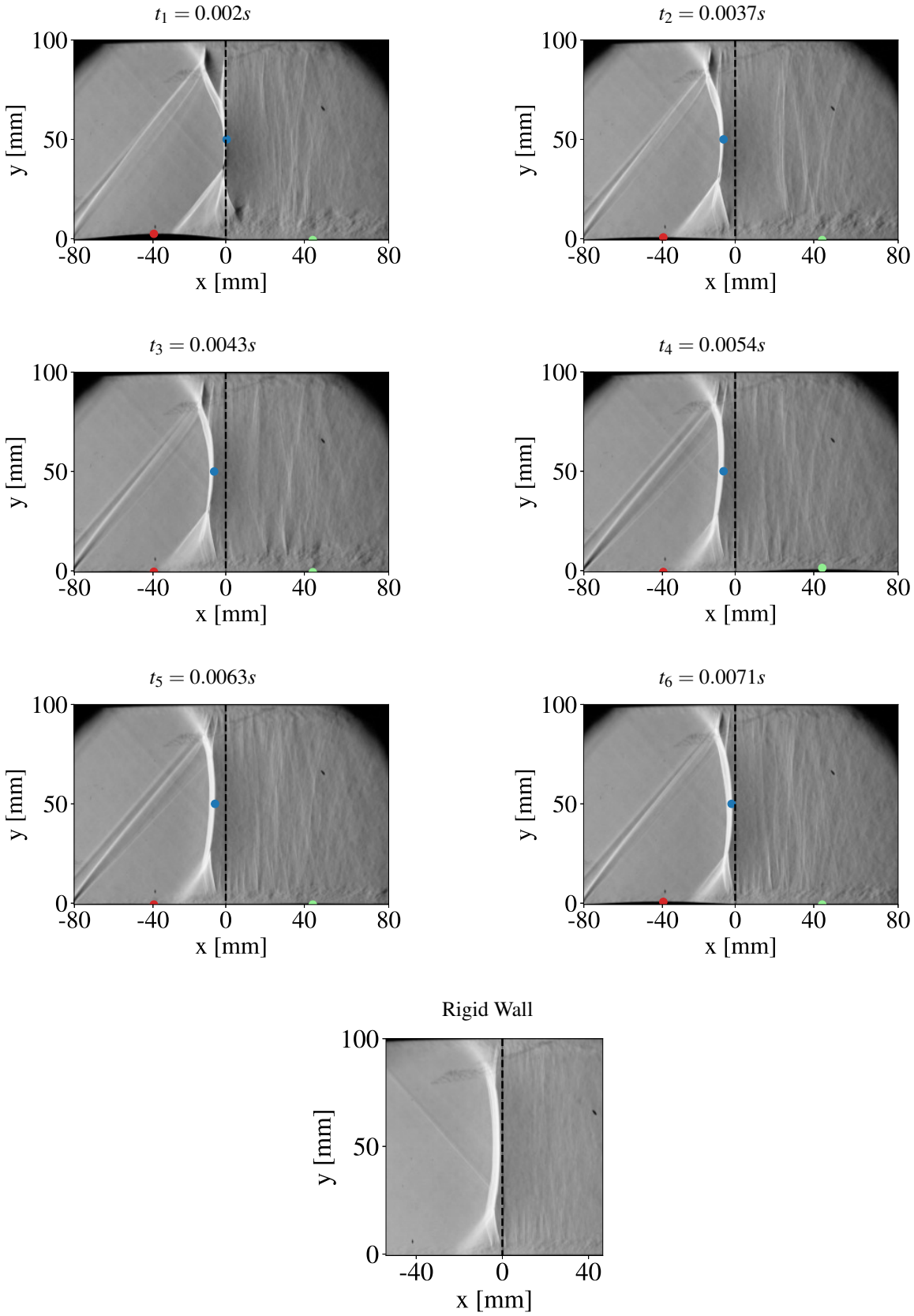

Figure 9: Instantaneous schlieren visualizations during a oscillation cycle of the compliant wall. Red, green and blue dots illustrate the displacement of the compliant wall and the shock. Last schlieren image corresponds to the rigid wall case.

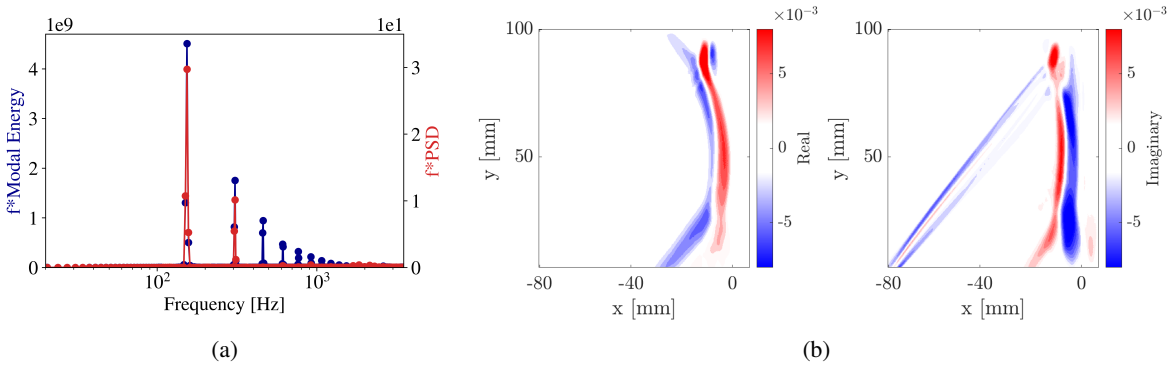

Figure 10: Spectral analysis of the compliant wall configuration. a) Premultiplied spectrum of (blue) the first SPOD eigenvalue of the schlieren vizualisation and (red) the compliant wall displacement at streamise location $x = -40$. b) Real (left) and imaginary (right) parts of the first mode at frequency 153 Hz

last schlieren image, at t_6, an upward deformation of the compliant wall is visible between x = -80 mm and x = 0 mm. This upward motion is accompanied by an downstream movement of the shock, which at t_6 is located at x = 0 mm. For the time being, at t_6, the shock still displays a similar λ region as shown at t_5. The results here presented suggest that there is a strong link between the motion of the compliant wall and the dynamics of the flow.

In order to better characterize that interaction, the frequency spectra of the flow and wall displacement are now analyzed and compared. The frequency content of the flow is first retrieved by performing a SPOD analysis on a set of schlieren images that exclude the wall. For this computation, 25 blocks of 2048 samples per block with 50% overlap are used. The blue line in Fig. 10a corresponds to the first eigenvalue of the SPOD analysis, premultiplied by the frequency. A dominant peak is clearly visible at $f = 153$ Hz and the other peaks of smaller magnitude corresponds to superharmonics, i.e. for frequencies $2f$, $3f$, ... The real and imaginary parts of the mode at $f = 153$ Hz, shown in Fig. 10b, both exhibit a change of sign upstream and downstream of the shock as well as at the shock foot. The opposite signs between the real and imaginary parts indicate that this mode is a standing wave creating an oscillation of the shock position after superposition with the time-averaged schlieren image. Note that the weak oblique shock, visible in the imaginary part of the mode as well as in the instantaneous images of Fig. 9, is due to a slight discontinuity of the rigid and compliant wall. It was also observed in other cases (not reported here) where the compliant wall does not display such large amplitude displacement so it has no major impact on the flow dynamics. From the schlieren SPOD analysis, we can finally conclude that the compliant wall strongly modifies the shock-wave dynamics since it oscillates periodically while it is characterized by a broadband frequency spectrum in the rigid wall case (see Fig. 5a).

The oscillation of the compliant wall is now analyzed by extracting from the schlieren images the y position of the red point in Fig. 9 that is located at $x = -40$, where the maximum upward deformation of the wall occurs. The power spectrum density of the extracted temporal signal is computed with a Welch method using 2048 samples per block with 50%overlap. The resulting premultiplied spectrum is shown with red lines in Fig. 10a. The largest amplitude peak is also found at 153 Hz, the same frequency as for the shock oscillation. This suggests that the shock-motion lock-in at the vibration frequency of the compliant wall.

To confirm the lock-in phenomenom, we determine the natural frequencies of the compliant wall by performing a finite-element modal analysis. The compliant structure, clamped at the four lateral boundaries and free to move at the bottom and top surfaces, is modeled with the three-dimensional linear elasticity equations. The vibration modes of lowest frequency, obtained by solving an eigenvalue problem, are shown in Fig. 11. The first, second and third modes oscillate at the natural frequencies 143 Hz, 182 Hz and 245 Hz, respectively. They display no spatial oscillation in the transverse direction (z) but have zero-node, one-nodes and two-nodes of oscillations in the streamwise direction (x). The frequency of the shock and compliant wall oscillations observed in the experiments is 153 Hz, so in between the first and second natural frequencies of the structure. Nonetheless, the displacement of the compliant wall observed in the experiments is closer to that of the second vibration mode. This is shown in Fig. 12, which displays the spatio-temporal evolution of the wall displacement at the centerline ($z = 0$) using a $x - t/T$ diagram. Fig. 12a corresponds to the second vibration mode (oscillating at 182 Hz) while the experimental results are shown in Fig. 12b.

The displacement of the second mode (Fig. 12a) exhibits an anti-symmetric pattern with respect to $x = 0$ that corresponds to the most upstream positions in the experiments as shown in Fig. 9 at t_1. For a fixed time, an upward displacement (red) of the compliant wall for $x < 0$ is asso-

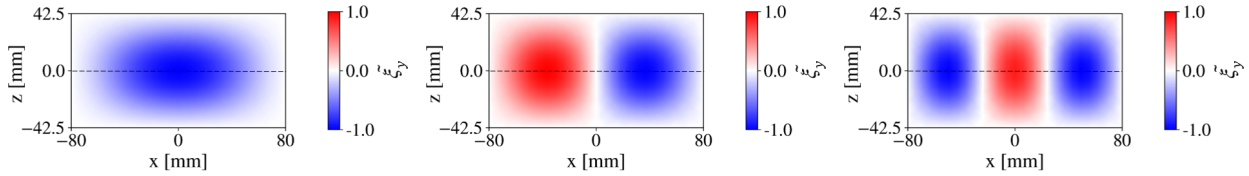

(a) f_1 = 143 Hz (b) f_2 = 182 Hz (c) f_3 = 245 Hz

Figure 11: Mode shapes of the first natural frequencies obtained with a finite-element modal analysis of the compliant wall structure.

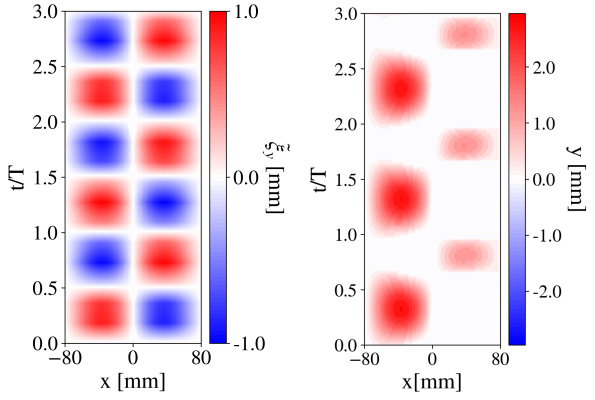

(a) (b)

Figure 12: Spatio-temporal evolution of the compliant wall displacement (a) of the second natural frequency mode vibrating at 182 Hz and (b) extracted from the schlieren vizualization and oscillating at 153 Hz. Negative displacement cannot be measured with our experimental set up.

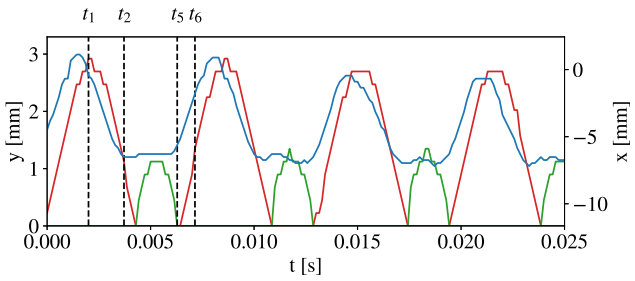

Figure 13: Displacement signals of the compliant wall at x = -43 mm (red) and x = 34 mm (green) and of the shock (blue).

ciated to an equal downward displacement for $x > 0$, and vice versa. For a fixed spatial position, let us say $x = -40$ where the largest amplitude is obtained, the wall displacement is alternatively positive and negative with identical extreme values. The wall displacements observed in the experiment (Fig. 12b) share some similarities with the pattern of the second mode. Upstream the shock position ($x < 0$), upwards displacement (red) are measured every half-period of oscillation. The downward displacement (blue) are not visible in the figure since they can not been measured from our schlieren visualization, but we may legitimately assume that white patterns correspond to negative displacements. Interestingly, downstream the shock $x > 0$, the upward displacement of the wall is of lower amplitude and for a shorter duration. This clearly indicates that, in the experiments, the compliant wall does not symmetrically oscillate around the $y = 0$ positions, but rather around a mean position that is below the $y = 0$ axis downstream the shock, and above that axis upstream the shock.

For a better picture of the fluid-structure interaction, the displacement signal at two points of the compliant wall, (Fig. 9, red and green dots) and at a point on the shock (Fig. 9, blue dot) are reported in Fig. 13. The points at the compliant wall correspond to the locations where the maximum displacement upstream and downstream are found, i.e. x = -43 mm and x = 34 mm. As all signals have been retrieved on the same set of images, they are synchronized and can be compared in time. As shown in Fig. 9, Fig. 13 illustrates an upward movement of the material upstream the shock coincides with a downstream translation of the shock and vice-versa. When the downstream part of the material presents an upward motion, the shock presents a small movement upstream, almost a plateau, as it is for the case between t_2 till t_5. This is consistent with the observation made in Fig. 9, where the shock seemed to remained in the same positions from t_2 till t_5. When looking at the signals, it is possible to see that the oscillation of the material presents a lag with respect to that of the shock. This implies that the most downstream position of the shock happens before the material has reached its maximum deformation. In order to asses the lag, the cross spectral density of both signals was computed. At the dominant frequency of the interaction, 153 Hz, the phase between both wall displacement signals and the shock signals is of 28 °.

5. CONCLUSION

The interaction of an unsteady normal shock with the incoming turbulent boundary layer has been experimentally characterised by unsteady pressure measurements and high speed schlieren visualizations. The pressure spectra showed that the shock oscillations ranged from 70 to 300 Hz, whereas oscillations related to the mixing layer ranged from 4 to 8 kHz. SPOD calculations were conducted on the schlieren videos. Low frequencies were related to modes associated to the displacement of the shock. High frequency associated modes displayed vortical structures shed downstream in the mixing layer. With SPOD it was also possible to find high frequency modes related to upstream traveling waves, which are thought to be of acoustic nature.

A compliant wall was chosen so that its natural frequencies are within the range of the shock oscillations. The fluid-structure interaction consists in a lock-in of the flow at the vibration frequency of the compliant wall. The dominant does not correspond to the natural frequencies of the unforced structure response. Nonetheless, the response of the compliant wall resembles the shape of the second mode. A further analysis of the response of the compliant wall to the forcing of the flow is needed. During the interaction, an upward deformation of the material coincides with an upstream displacement of the shock. A cross spectral analysis showed that the movement of the shock and the compliant wall are out of phase.

6. ACKNOWLEDGEMENTS

This work is co-funded by the Direction Générale de l'Armement (AID Convention N° 2020 65 0022) and ONERA.

REFERENCES

[1] Y.-J. Ahn, M.A. Eitner, M.N. Musta, S. Rafati, J. Sirohi, and N.T. Clemens. Experimental Investigation of Flow-Structure Interaction of a Compliant Panel under Mach 2 Compression-Ramp Interaction. *AIAA Science and Technology Forum and Exposition, AIAA SciTech Forum 2022*, 2022.

[2] H. Babinsky and J. K. Harvey. *Shock Wave-Boundary-Layer Interactions*. Cambridge Aerospace Series. Cambridge University Press, 2011.

[3] K.R. Brouwer, R.A. Perez, T.J. Beberniss, S.M. Spottswood, and D.A. Ehrhardt. Experiments on a Thin Panel Excited by Turbulent Flow and Shock/Boundary-Layer Interactions. *AIAA Journal*, 59(7):2737–2752, 2021.

[4] P.J.K. Bruce and H. Babinsky. Unsteady shock wave dynamics. *Journal of Fluid Mechanics*, 603:463–473, 2008.

[5] R. Bur, R. Benay, A. Galli, and P. Berthouze. Experimental and numerical study of forced shock-wave oscillations in a transonic channel. *Aerospace Science and Technology*, 10(4):265–278, 2006.

[6] R. Bur, B. Corbel, and J. Delery. Study of passive control in a transonic shock wave/boundary-layer interaction. *AIAA Journal*, 36(3):394–400, 1998.

[7] N.T. Clemens and V. Narayanaswamy. Low-frequency unsteadiness of shock wave/turbulent boundary layer interactions. *Annual Review of Fluid Mechanics*, 46:469–492, 2014.

[8] P. Dupont, C. Haddad, J.P. Ardissone, and J.F. Debiève. Space and time organisation of a shock wave/turbulent boundary layer interaction. *Aerospace Science and Technology*, 9(7):561–572, oct 2005.

[9] J.A. Edwards and L.C. Squire. An experimental study of the interaction of an unsteady shock with a turbulent boundary layer at Mach numbers of 1.3 and 1.5. *Aeronautical Journal*, 11(1):93–118, 1992.

[10] M.A. Eitner, Y.-J. Ahn, L. Vanstone, M.N. Musta, J. Sirohi, and N.T. Clemens. Effect of Shock-Wave Boundary Layer Interaction on Vibratory Response of Compliant Panel. *AIAA SciTech Forum 2021*, pages 1–18, 2021.

[11] M.E. Erengil and D.S. Dolling. Unsteady wave structure near separation in a Mach 5 compression rampinteraction. *AIAA Journal*, 29(5):728–735, 1991.

[12] M. Gramola, P. J.K. Bruce, and M. Santer. Off-design performance of 2D adaptive shock control bumps. *Journal of Fluids and Structures*, 93:102856, 2020.

[13] M. Gramola, P.J.K. Bruce, and M. Santer. Experimental FSI study of adaptive shock control bumps. *Journal of Fluids and Structures*, 81:361–377, 2018.

[14] E. Jinks, P. Bruce, and M. Santer. Wind tunnel experiments with flexible plates in transonic flow. *54th AIAA Aerospace Sciences Meeting*, pages 1–18, 2016.

[15] M.N. Musta, L. Vanstone, Y.-J. Ahn, M. Eitner, J. Sirohi, and N. Clemens. Investigation of flow-structure coupling for a compliant panel under a shock/boundary-layer interaction using fast-response PSP. *AIAA SciTech Forum 2021*, pages 1–16, 2021.

[16] F. Sartor, C. Mettot, R. Bur, and D. Sipp. Unsteadiness in transonic shock-wave/boundary-layer interactions: experimental investigation and global stability analysis. *Journal of Fluid Mechanics*, 781:550–577, 2015.

[17] A. Towne, O.T. Schmidt, and T. Colonius. Spectral proper orthogonal decomposition and its relationship to dynamic mode decomposition and resolvent analysis. *Journal of Fluid Mechanics*, 847:821–867, 2018.

[18] A. Tripathi, J. Gustavsson, K. Shoele, and R. Kumar. Response of a compliant panel to shock boundary layer interaction at mach 2. *AIAA Scitech 2021 Forum*, pages 1–15, 2021.

[19] S.V. Varigonda, V. Narayanaswamy, and I. Boxx. Investigations of fsi generated by an impinging sbli on a thin panel using multivariate imaging of flow/structural properties. *AIAA Aviation 2020 Forum*, 1 PartF:1–20, 2020.